Asociación Argentina
de Mecánica Computacional

Mecánica Computacional Vol XXX, págs. 675-688 (artículo completo)
Oscar Möller, Javier W. Signorelli, Mario A. Storti (Eds.)
Rosario, Argentina, 1-4 Noviembre 2011

DISCONTINUOUS BIFURCATION ANALYSIS IN THE PERFORMANCE DEPENDENT MODEL FOR CONCRETE

Paula Folino[a], Sonia Vrech[b] and Guillermo Etse[a,b]

[a] *LMNI - Laboratorio de Métodos Numéricos en Ingeniería- Laboratorio de Materiales y Estructuras - INTECIN- Facultad de Ingeniería - Universidad de Buenos Aires - Las Heras 2214 (C1127AAR) - Buenos Aires - Argentina - pfolino@fi.uba.ar*

[b] *CEMCI - Centro de Métodos Numéricos y Computacionales en Ingeniería Facultad de Ciencias Exactas y Tecnología - Universidad de Nacional Tucumán - Av. Independencia 1800 (CP 4000) - Tucumán - Argentina - SVrech@herrera.unt.edu.ar*

Keywords: discontinuous bifurcation, failure modes, acoustic tensor, high strength concrete.

Abstract. This paper presents the predictions of different failure modes when concretes of arbitrary strength are subjected to different load scenarios. The discontinuous bifurcation analysis is performed in the Performance Dependent Model for concretes recently proposed by two of the authors, a constitutive formulation valid for both normal and high strength concretes. Based on the incremental flow theory of plasticity, it depends on the three stress invariants, its maximum strength surface is defined by the Performance Dependent Failure Criterion, including a non uniform hardening law, an isotropic fracture energy based softening law and following a volumetric non associative flow rule.
Analytical and geometrical localization analysis is applied particularly for the case of uniaxial compression, based on the properties of the acoustic tensor. The results demonstrate the incidence of the relative brittleness of high strength concretes into the failure behavior in comparison with normal strength concretes.

1 INTRODUCTION

Recent advances in the field of concrete technology have led to the development of high strength concretes (HSC) which present a mechanical behavior that substantially differs from that of normal strength concretes (NSC). (See e.g. van Mier (1997), Xie et al. (1995), etc.). Experimental evidence demonstrates that among other differences, behavior both in pre and post peak regimes is considerably more brittle in the case of HSC under different loading paths.
Regarding this, the aim of this work is to analyze the incidence of concrete quality in the failure mode. Although several authors have studied localization characteristics based on concrete constitutive models, none of these works was focused on concrete quality. (See a.o. Etse (1992a), Kang and Willam (1999), Vrech (2007)).
The localization analysis presented in this paper is based on the Performance Dependent Model (PDM) recently developed, formulated in terms of concrete quality by the dependence on the performance parameter β_P, an index that together with the uniaxial compressive strength $f_c^{'}$ define concrete quality. (See Folino et al. (2009) and Folino and Etse (2011)).
The PDM, valid for plain concretes in the range of $f_c^{'}$ from 20 to 120 MPa, is based on the flow theory of plasticity, it depends on the three stress invariants, and its maximum strength surface is defined by the Performance Dependent Failure Criterion (PDFC). It considers a non uniform hardening law and an isotropic softening rule defined in terms of the concrete quality and of the first invariant of stresses in order to consider the influence of confinement on the ductility in the pre and post peak responses. Softening law is based on fracture energy concepts. It considers a volumetric non associative flow rule.
The localization analyses are performed based on both the analytical solution of the discontinuous bifurcation condition and on the geometrical method. The results demonstrate the capabilities of the PDM to capture the different failure characteristics of NSC and HSC.

2 LOCALIZATION CONDITION

Localized failure (or weak discontinuity) is characterized by a jump in the strains field $\underline{\underline{\dot{\varepsilon}}}$, being still continuous the displacement field $\underline{\dot{u}}$. It is associated with the loss of ellipticity of the governing equilibrium equations and has a clear preferred failure plane orientation, and may occur prior or after the peak stress.
Localized failure: $[\![\underline{\dot{u}}]\!] = \underline{\mathbf{0}}$; $[\![\underline{\underline{\dot{\varepsilon}}}]\!] \neq \underline{\underline{\mathbf{0}}}$
The localization condition may be derived based on the works by Rudnicki and Rice (1975) and and Rice (1976), which in turn are based on previous developed theories by Hadamard (1903) and Hill (1962). The point of departure of these works is the analogy observed between the propagation of acoustic plane waves in solids and the propagation of a displacement field rate, when a discontinuity is found. In this case, the wave speed becomes null. (See a.o. Ortiz (1987) and Willam (2002)).
The jump condition in the strains field can be expressed applying the Maxwell's compatibility condition (Truesdell and Toupin (1960)), representing the velocity gradient as a rank one tensor

$$[\![\underline{\nabla}\ \underline{\dot{u}}]\!] = \dot{\gamma}\ \underline{M}\ \underline{N} \tag{1}$$

In the above equation, the strains rate jump is represented by the product of two unit vectors: $\underline{M}$ representing the motion direction of the points, and $\underline{N}$ defined as the direction of the normal of the failure plane. The scalar magnitude $\dot{\gamma}$ is the amplitude of the jump.

In the case of infinitesimal strains, Eq. 1 implies that the strains rate jump derives in

$$\left[\left[\underline{\dot{\boldsymbol{\varepsilon}}}\right]\right] = \left[\left[\underline{\nabla}^s \, \underline{\dot{\boldsymbol{u}}}\right]\right] = \dot{\gamma} \, (\underline{\boldsymbol{M}} \, \underline{\boldsymbol{N}})^{sym} = \frac{1}{2} \, \dot{\gamma} \, (\underline{\boldsymbol{M}} \, \underline{\boldsymbol{N}} + \underline{\boldsymbol{N}} \, \underline{\boldsymbol{M}}) \tag{2}$$

The constitutive model for concretes considered in this paper is based on the elastoplastic incremental nonassociative flow theory and the smeared crack approach. Post peak behavior of concrete is modeled by a fracture energy based softening law.
Only infinitesimal strains are admitted. Elastic-plastic coupling is neglected, accepting the additive Prandtl-Reuss decomposition of the infinitesimal strain rate tensor into its elastic and plastic parts. The constitutive model is the represented by the following equation

$$\underline{\dot{\boldsymbol{\sigma}}} = \underline{\underline{\boldsymbol{E}}}^{EP} : \underline{\dot{\boldsymbol{\varepsilon}}} \tag{3}$$

whereby the material elastoplastic operator is

$$\underline{\underline{\boldsymbol{E}}}^{EP} = \underline{\underline{\boldsymbol{E}}} - \frac{\underline{\underline{\boldsymbol{E}}} : \underline{\boldsymbol{m}} \;\; \underline{\boldsymbol{n}} : \underline{\underline{\boldsymbol{E}}}}{\underline{\boldsymbol{n}} : \underline{\underline{\boldsymbol{E}}} : \underline{\boldsymbol{m}} + \underline{\boldsymbol{H}} : \underline{\boldsymbol{m}}} \tag{4}$$

In the above equations, $\underline{\dot{\boldsymbol{\sigma}}}$ is the Cauchy stress rate tensor, $\underline{\underline{\boldsymbol{E}}}$ is the fourth order elasticity tensor, $\underline{\boldsymbol{n}}$ is the gradient to the yield surface denoted as f, limiting the actual elastic range, which size and shape depend on a set of state variables q, and $\underline{\boldsymbol{m}}$ is the gradient of the plastic potential surface g which does not coincide with f. Inelastic material response is governed, by the following non associated flow rule

$$\underline{\dot{\boldsymbol{\varepsilon}}}^P = \underline{\boldsymbol{m}} \, \dot{\lambda} \tag{5}$$

The scalar magnitude resulting from the double contraction of the tensors $\underline{\underline{\boldsymbol{H}}}$ (hardening tensor) and $\underline{\boldsymbol{m}}$ is known as hardening modulus h_p

$$h_p = \underline{\underline{\boldsymbol{H}}} \;\; : \;\; \underline{\boldsymbol{m}} \tag{6}$$

In order to satisfy equilibrium condition, the jump in the traction vector must be null. After applying Cauchy′s theorem, the equilibrium condition turns to

$$\left[\left[\underline{\dot{\boldsymbol{t}}}\right]\right] = \underline{\boldsymbol{0}} \;\; \Rightarrow \;\; \underline{\boldsymbol{N}} \cdot \left[\left[\underline{\dot{\boldsymbol{\sigma}}}\right]\right] = \underline{\boldsymbol{N}} \cdot \left[\left[\underline{\underline{\boldsymbol{E}}}^{EP} : \underline{\dot{\boldsymbol{\varepsilon}}}\right]\right] = \underline{\boldsymbol{0}} \tag{7}$$

Assuming that the elastoplastic operator is the same at both sides of the failure plane, and applying the symmetry of the strain tensor, the last equation leads to

$$\underline{\boldsymbol{N}} \cdot \underline{\underline{\boldsymbol{E}}}^{EP} : \left[\left[\underline{\dot{\boldsymbol{\varepsilon}}}\right]\right] = \underline{\boldsymbol{N}} \cdot \underline{\underline{\boldsymbol{E}}}^{EP} : \dot{\gamma} \, (\underline{\boldsymbol{N}} \, \underline{\boldsymbol{M}}) = \dot{\gamma} \, (\underline{\boldsymbol{N}} \cdot \underline{\underline{\boldsymbol{E}}}^{EP} \cdot \underline{\boldsymbol{N}}) \cdot \underline{\boldsymbol{M}} = \underline{\boldsymbol{0}} \tag{8}$$

Defining the acoustic or localization elastoplastic tensor as

$$\underline{\underline{\boldsymbol{Q}}}^{EP} = \underline{\boldsymbol{N}} \cdot \underline{\underline{\boldsymbol{E}}}^{EP} \cdot \underline{\boldsymbol{N}} \tag{9}$$

It may be observed that the localization equation (Eq. 8) takes an eigenvalue problem form, and consequently, the localization condition is

$$\det \left[\underline{\underline{\boldsymbol{Q}}}^{EP}\right] \doteq 0 \Rightarrow \;\; \lambda_{min} \left(\underline{\underline{\boldsymbol{Q}}}^{EP}\right) = 0 \tag{10}$$

During the loading process and before the hardening begins, the behavior is supposed to be elastic, and the corresponding elastic acoustic tensor takes the form

$$\underline{\underline{\boldsymbol{Q}}}^{E} = \underline{\boldsymbol{N}} \cdot \underline{\underline{\underline{\underline{\boldsymbol{E}}}}} \cdot \underline{\boldsymbol{N}} \tag{11}$$

With this definition and considering the elastoplastic material tensor according to Eq. 4, then the elastoplastic acoustic tensor may be expressed as the degradation of the elastic acoustic tensor as follows

$$\underline{\underline{\boldsymbol{Q}}}^{EP} = \underline{\underline{\boldsymbol{Q}}}^{E} - \frac{(\underline{\boldsymbol{N}} \cdot \underline{\underline{\underline{\underline{\boldsymbol{E}}}}} : \underline{\underline{\boldsymbol{m}}}) \ (\underline{\boldsymbol{n}} : \underline{\underline{\underline{\underline{\boldsymbol{E}}}}} \cdot \underline{\boldsymbol{N}})}{\underline{\boldsymbol{n}} : \underline{\underline{\underline{\underline{\boldsymbol{E}}}}} : \underline{\underline{\boldsymbol{m}}} + \underline{\underline{\boldsymbol{H}}} : \underline{\underline{\boldsymbol{m}}}} \tag{12}$$

The above equation may be expressed as

$$(\underline{\underline{\boldsymbol{Q}}}^{E})^{-1} : \underline{\underline{\boldsymbol{Q}}}^{EP} = 1 - (\underline{\underline{\boldsymbol{Q}}}^{E})^{-1} : \frac{(\underline{\boldsymbol{N}} \cdot \underline{\underline{\underline{\underline{\boldsymbol{E}}}}} : \underline{\underline{\boldsymbol{m}}}) \ (\underline{\boldsymbol{n}} : \underline{\underline{\underline{\underline{\boldsymbol{E}}}}} \cdot \underline{\boldsymbol{N}})}{\underline{\boldsymbol{n}} : \underline{\underline{\underline{\underline{\boldsymbol{E}}}}} : \underline{\underline{\boldsymbol{m}}} + \underline{\underline{\boldsymbol{H}}} : \underline{\underline{\boldsymbol{m}}}} \tag{13}$$

Turning the localization condition to

$$\det \left[(\underline{\underline{\boldsymbol{Q}}}^{E})^{-1} : \underline{\underline{\boldsymbol{Q}}}^{EP} \right] \doteq 0 \ \Rightarrow \ \det \left[\underline{\underline{\boldsymbol{Q}}}^{EP} \right] \ / \ \det \left[\underline{\underline{\boldsymbol{Q}}}^{E} \right] \doteq 0 \tag{14}$$

The loss of strong ellipticity, defined by

$$\det \left[\underline{\underline{\boldsymbol{Q}}}^{EPsym} \right] \ / \ \det \left[\underline{\underline{\boldsymbol{Q}}}^{E} \right] \doteq 0 \tag{15}$$

may occur prior to the loss of ellipticity. This may be demonstrated by applying Bromwich eigenvalue bounds of non-symmetric matrices, which conduces to

$$\lambda_{min} \left(\underline{\underline{\boldsymbol{Q}}}^{EPsym} \right) \leq \lambda \left(\underline{\underline{\boldsymbol{Q}}}^{EP} \right) \leq \lambda_{max} \left(\underline{\underline{\boldsymbol{Q}}}^{EPsym} \right) \tag{16}$$

The smallest eigenvalue of $\underline{\underline{\boldsymbol{Q}}}^{EPsym}$ with respect to the metric defined by $\left(\underline{\underline{\boldsymbol{Q}}}^{E} \right)^{-1}$

$$\lambda_{min} = 1 - \frac{\underline{\boldsymbol{a}}_n \cdot \left(\underline{\underline{\boldsymbol{Q}}}^{E} \right)^{-1} \cdot \underline{\boldsymbol{a}}_m}{\underline{\boldsymbol{n}} : \underline{\underline{\underline{\underline{\boldsymbol{E}}}}} : \underline{\underline{\boldsymbol{m}}} + \underline{\underline{\boldsymbol{H}}} : \underline{\underline{\boldsymbol{m}}}} = 0 \tag{17}$$

with

$$\underline{\boldsymbol{a}}_m = \underline{\boldsymbol{N}} \cdot \underline{\underline{\underline{\underline{\boldsymbol{E}}}}} : \underline{\underline{\boldsymbol{m}}} \quad , \quad \underline{\boldsymbol{a}}_n = \underline{\boldsymbol{n}} : \underline{\underline{\underline{\underline{\boldsymbol{E}}}}} \cdot \underline{\boldsymbol{N}} \tag{18}$$

leads to the localization condition

$$\underline{\underline{\boldsymbol{H}}} : \underline{\underline{\boldsymbol{m}}} + \underline{\boldsymbol{n}} : \underline{\underline{\underline{\underline{\boldsymbol{E}}}}} : \underline{\underline{\boldsymbol{m}}} - \underline{\boldsymbol{a}}_n \cdot \left(\underline{\underline{\boldsymbol{Q}}}^{E} \right)^{-1} \cdot \underline{\boldsymbol{a}}_m = 0 \tag{19}$$

This equation serves as a basis for analytical, numerical and geometrical evaluations of the critical parameters corresponding to discontinuous biburcation and their associated localization directions $\underline{\boldsymbol{N}}$.

Analytical explicit solutions for classical plasticity were developed by Ottosen and Runesson (1991) and by Perić (1990), for tridimensional stress states and plane states, respectively. For the special case of quasi-brittle materials analytical solutions were developed by Etse (1992a) and Etse (1992b).

3 GEOMETRICAL METHOD

Geometrical methods for localization analysis follows the original proposal by Benallal (1992), Pijaudier-Cabot and Benallal (1993) and Benallal and Comi (1996). The localization condition in Eq. (19) defines an ellipse

$$\frac{(\sigma-\sigma_0)^2}{X^2}-\frac{\tau^2}{Y^2}=1 \tag{20}$$

in the $\sigma-\tau$ Mohr's coordinates

$$\sigma=\underline{\boldsymbol{N}}\cdot\underline{\underline{\boldsymbol{\sigma}}}\cdot\underline{\boldsymbol{N}} \quad , \quad s=\underline{\boldsymbol{N}}\cdot\underline{\underline{\boldsymbol{S}}}\cdot\underline{\boldsymbol{N}} \tag{21}$$

$$\tau=(\underline{\boldsymbol{N}}\cdot\underline{\underline{\boldsymbol{S}}})\cdot(\underline{\boldsymbol{N}}\cdot\underline{\underline{\boldsymbol{S}}})-(\underline{\boldsymbol{N}}\cdot\underline{\underline{\boldsymbol{S}}}\cdot\underline{\boldsymbol{N}})^2 \tag{22}$$

being $\underline{\underline{\boldsymbol{S}}}$ the deviatoric stress tensor and $\underline{\boldsymbol{N}}$ the normal to the plane where the Mohr components are evaluated.

The maximum hardening/softening parameter $\bar{H}_c=\underline{\underline{\boldsymbol{H}}}:\underline{\underline{\boldsymbol{m}}}$ and the critical directions θ_c for localization are obtained when the Mohr circle of stresses

$$(\sigma-\sigma_c)^2+\tau^2=R^2 \tag{23}$$

contacts the elliptical localization envelope, being center and radius of the Mohr circle in Eq. (23)

$$\sigma_c=\frac{\sigma_1+\sigma_3}{2} \quad \text{and} \quad R=\frac{\sigma_1-\sigma_3}{2} \tag{24}$$

According to Liebe (1998) three different failure modes may be distinguished depending on the contact points location: mode I, mode II and mixed mode. The interrelationship between the radius R of the Mohr's Circle and the curvature of the localization ellipse ρ^e

$$\rho^e_{min}\le\rho^e\le\rho^e_{max}, \quad \text{being} \quad \rho^e_{min}=\frac{Y^2}{X} \quad , \quad \rho^e_{max}=Y \tag{25}$$

give the three different failure modes

- *Failure Mode I*: $R\le\rho^e_{min}$, $\theta_c=0^\circ$
- *Failure Mode II*: $R\le\rho^e_{max}$, $\theta_c=45^\circ$
- *Mixed Failure Mode*: $R>\rho^e_{min}$, $2\theta_c\neq 90^\circ$

4 PERFORMANCE DEPENDENT MODEL FOR CONCRETES (PDM)

In this section a brief description of the PDM is presented. For further details see Folino and Etse (2010).

4.1 Maximum strength criterion for concretes of arbitrary strength

The performance dependent failure criterion (PDFC), valid both for normal and high strength concretes, is adopted as maximum strength surface. Defined in the Haigh Westergaard stress space in terms of the normalized stress coordinates (with respect to $f_c{}'$) $\overline{\xi}$, $\overline{\rho}$ and θ, depends on

the three stress invariants I_1, J_2 and J_3.
The compressive and tensile meridians are defined by two parabolic equations

$$\theta = \frac{\pi}{3} \Rightarrow A\,\overline{\rho_c^*}^2 + B_c\,\overline{\rho_c^*} + C\,\overline{\xi} - 1 = 0 \tag{26}$$

$$\theta = 0 \Rightarrow A\,\overline{\rho_t^*}^2 + B_t\,\overline{\rho_t^*} + C\,\overline{\xi} - 1 = 0 \tag{27}$$

In the previous equations, the upper asterisk denotes failure, the subscripts "c" and "t" indicate compressive and tensile meridians respectively.
In the deviatoric plane, the elliptic interpolation between the compressive and the tensile meridians by Willam and Warnke (1974) is followed.

$$\forall\, 0^0 \leqslant\ \theta\ \leqslant 60^0\ \Rightarrow\ \overline{\rho^*} = \frac{\overline{\rho_c^*}}{r} \tag{28}$$

The ellipticity factor r is defined as

$$r = \frac{4(1-e^2)\cos^2\theta + (2e-1)^2}{2(1-e^2)\cos\theta + (2e-1)\sqrt{4(1-e^2)\cos^2\theta + 5e^2 - 4e}} \tag{29}$$

where e is the eccentricity $\overline{\rho_t^*}/\overline{\rho_c^*}$.
The above equations lead to the general unified quadratic expression representing the failure surface

$$F_{max} = A\,r^2\,\overline{\rho^*}^2 + B_c\,r\,\overline{\rho^*} + C\,\overline{\xi} - 1 = 0 \tag{30}$$

Coefficients A, B_c, B_t, and C defining the main meridians, are functions of four material properties, leading to different failure surfaces that depend on the concrete quality. The involved material parameters are: the uniaxial compressive strength $f_c{}'$, the uniaxial tensile strength ratio $\alpha_t = f_t{}'/f_c{}'$, the biaxial compressive strength ratio $\alpha_b = f_b{}'/f_c{}'$ (being $f_b{}'$ the biaxial compressive strength), and a parameter m representing the friction defined as the tangent to the compressive meridian on the peak stress's shear component corresponding to the uniaxial compression test. Considering that three of the involved material properties are obtained from non standard and complex experimental tests, and that those properties depends on the concrete composition, internal functions were proposed to determine these properties in terms of two fundamental parameters: $f_c{}'$ and the performance parameter β_P. The latter is an index that together with $f_c{}'$ define concrete quality. It is defined as

$$\beta_P = \frac{1}{1000}\frac{f_c'}{(w/b)} \qquad f_c' \text{ in } [\text{MPa}] \tag{31}$$

where w/b is the water-binder ratio, being W the water content and B the binder content, both in [kg/m3]. The binder is constituted by the sum of the cement and the mineral admixtures contents.
Parameter β_P varies approximately between 0 and 1. A greater value of β_P means a more homogeneous concrete with less porosity. (See Folino et al. (2009) and Folino and Etse (2011) for further details).

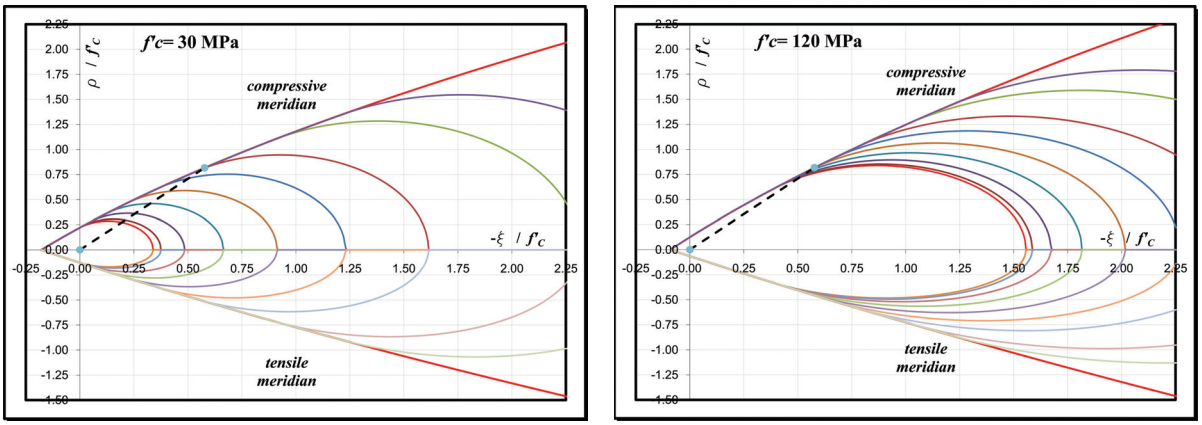

(a) (b)

Figure 1: Compressive and tensile meridian views of the loading surfaces in hardening for (a) NSC and (b) HSC

4.2 Pre peak regime

4.2.1 Loading surfaces in pre peak regime

In the PDM the successive loading surfaces are of the type so-called "cone and cap" or "cap plasticity". (See Fig. 1). Consequently, each loading surface is composed by two different surfaces with a common deviatoric plane. The first one, representing the cone, is the failure surface defined by Eq. 30. The second one, is a compressive cap defined by elliptical meridians centered over the hydrostatic axis. The common deviatoric plane is defined by the hydrostatic coordinate of a point denoted as "P1" at which a continuity of type C^1 is observed. During the hardening process, "P1" will continuously change, leading to a non uniform hardening.

Since point "P1" lies on the maximum strength surface, its coordinates on the compressive meridian $(\overline{\xi}_1; \overline{\rho}_{c1})$ are related by $\overline{\xi}_1 = (1 - A\,(\overline{\rho}_{c1})^2 - B_c\,\overline{\rho}_{c1})\,/C$. Each loading surface is associated to a hardening level parameter k defined in terms of the $\overline{\rho}_{c1}$ coordinate of point "P1" as

$$k = \frac{\overline{\rho}_{c1}}{\sqrt{2/3}} \tag{32}$$

This parameter has a minimum initial value k_o corresponding to the first loading surface where the inelastic behavior starts, and depending on the concrete quality. Nevertheless, it has no upper limit, indicating that ideally the loading surfaces can evolve indefinitely. The successive surfaces are mathematically defined as

$$f_h = \begin{cases} f_h^{cone} = F_{\max} = A\,r^2\,\overline{\rho*}^2 + B_c\,r\,\overline{\rho*} + C\,\overline{\xi} - 1 = 0 & \text{if } \overline{\xi} \leqslant \overline{\xi}_{1(k)} \\ f_{h(k)}^{cap} = \dfrac{\left(\overline{\xi} - \overline{\xi}_{cen(k)}\right)^2}{a_{(k)}^2} + \dfrac{r^2\,\overline{\rho}^2}{b_{(k)}^2} - 1 = 0 & \text{if } \overline{\xi} > \overline{\xi}_{1(k)} \end{cases} \tag{33}$$

The dimensions and location of the elliptical cap are defined by the coefficients a (ellipse semi-axis on the hydrostatic axis), b (ellipse semi-axis on the deviatoric axis) and $\overline{\xi}_{cen}$ (coordinate of the center of the ellipse on the hydrostatic axis), all of them depending on k. These coefficients are defined departing from the corresponding to the initial loading surface. The ratio between the two ellipse semi axes remains constant ($R_{ab} = a^2/b^2$). (See Folino and Etse (2008)).

The final expressions of the ellipses parameters are the following

$$\overline{\xi}_{cen(k)} = \frac{1}{C}\left[1 - A\frac{2}{3}k^2 - B_c\sqrt{\frac{2}{3}}k - \sqrt{\frac{2}{3}}\frac{C^2 R_{ab}}{2Ak\sqrt{2/3} + B_c}k\right] \tag{34}$$

$$a^2_{(k)} = \left[\frac{1}{C}\left(1 - \frac{2}{3}Ak^2 - \sqrt{\frac{2}{3}}B_c k\right) - \overline{\xi}_{cen(k)}\right]^2 + \frac{2}{3}R_{ab}k^2 \tag{35}$$

$$b^2_{(k)} = a^2_{(k)}/R_{ab} \tag{36}$$

4.2.2 Hardening law

The evolution of the hardening parameter is defined as

$$k = k_o + (k_{max} - k_o)\sqrt{\kappa_h\,(2 - \kappa_h)} \tag{37}$$

where k_{max} is derived from the definition of k, considering the hardening parameter associated with the largest ellipse possible for a given value of confinement $\bar{\xi}$, and κ_h is a normalized work hardening measure defined as the ratio between the actual developed work hardening $\dot{\omega}_a^P$, and the total work hardening capacity W_t^P for the actual confinement level $\bar{\xi}$

$$\dot{\kappa_h} = \frac{\dot{\omega}_a^P}{W_t^P} = \frac{\underline{\underline{\boldsymbol{\sigma}}} : \underline{\underline{\boldsymbol{m}}}\,\dot{\lambda}}{W_t^P} \tag{38}$$

While variable $\dot{\omega}_a^P$ is continuously updated during the calculation process, W_t^P is an unknown since the maximum plastic strain $\varepsilon^P_{\max}$ for the actual confinement is still unknown during the inelastic process. In the PDM this variable is evaluated by the following expression

$$W_t^P \begin{cases} = E^{wpt}_{(\beta_P, f'_c)}\left(\overline{\xi} - \overline{\xi}_{P1o}\right)\left[f_1 + f_2\left(\overline{\xi} - \overline{\xi}_{P1o}\right)^6\right] & \text{if } \ \overline{\xi} \geqslant \overline{\xi}_{lim} \\ = f_3\,\overline{\xi}^2 + f_4\,\overline{\xi} + f_5 & \text{if } \ \overline{\xi} < \overline{\xi}_{lim} \end{cases} \tag{39}$$

Where f_i, $\overline{\xi}_{lim}$ and E_{wpto} are in turns functions depending on the material quality.

4.3 Post peak regime

4.3.1 Unloading surfaces in post peak regime

An isotropic softening is adopted represented by the continuous contraction of the cone. Each surface is associated to a softening parameter c representing the decohesion. It represents the ratio between the actual and the maximum strength property both under mode I and II type of softening processes. Consequently, it varies between a maximum value c=1 at peak strength, before activating the degradation or softening process in the material, and a minimum value $c = \sigma_{res}/\sigma_{max}$, being σ_{res} the residual strength and σ_{max}, the maximum one.
The unloading surfaces are mathematically described as (See Fig. 2)

$$f_s = A\,r^2\,\overline{\rho}^2 + B_c\,r\,\overline{\rho} + C\,\overline{\xi} - c = 0 \tag{40}$$

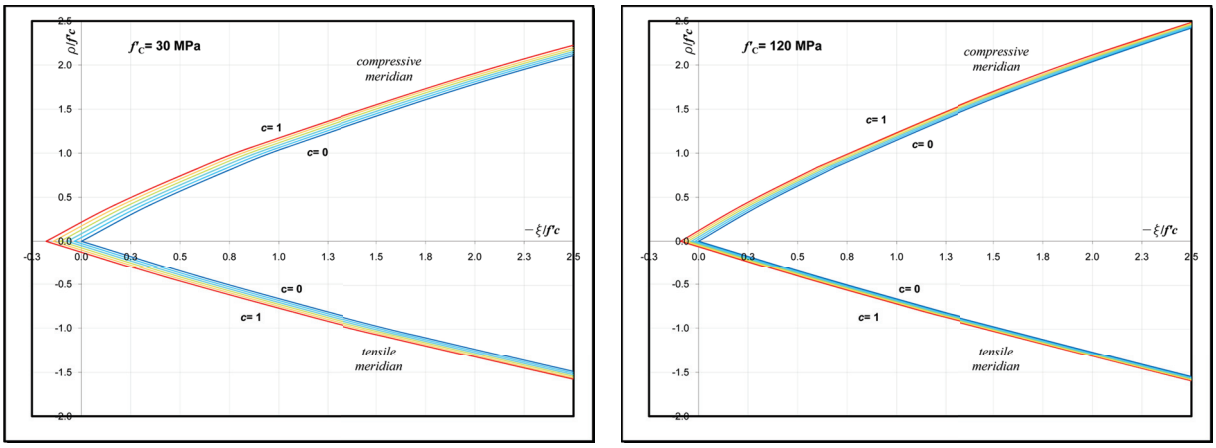

(a) (b)

Figure 2: Post peak unloading surfaces (a) NSC and (b) HSC

4.3.2 Fracture energy based softening law

Fracture energy properties are incorporated in the $\boldsymbol{\sigma}$-$\boldsymbol{\varepsilon}$ relation by introducing an homogenization strategy. Fracture energy G_f^I dissipated during the crack opening process along the surface of the crack A_t in a direct tensile test, is considered to be equal to the energy W dissipated during plastic softening in the continuum

$$\begin{cases} dG_f^I \; A_t = \displaystyle\int_{A_t} \boldsymbol{\sigma}_t \; du_f \; dA \\ \\ dW_f = \displaystyle\int_{V_t} \boldsymbol{\sigma}_t \; d\widetilde{\varepsilon}_f \; dV \end{cases} \tag{41}$$

Crack opening displacement $\dot{u}_f$ is evaluated by the consideration of equivalent tensile fracture strains $\dot{\widetilde{\varepsilon}}_f$ uniformly distributed in the continuum in a localization width l_c which constitutes an internal characteristic length

$$\dot{u}_f = l_c \; \dot{\widetilde{\varepsilon}}_f \tag{42}$$

In this case (mode I), the characteristic length l_c is a measure of the crack spacing in a direct tensile test h_t. If the same concept is now extended to a general mode II of failure, then the corresponding fracture energy in mode II, G_f^{II} must be considered, and an appropriate characteristic length should be adopted.
The evolution of the softening parameter is defined as

$$c = \exp\left(\frac{-\delta \; \kappa_s}{u_r}\right) \tag{43}$$

where u_r represents the maximum crack opening displacement, δ is a parameter that defines the shape of the decay function, and κ_s is a fracture energy based softening measure defined as follows

$$\dot{\kappa}_s = l_c \; \dot{\widetilde{\varepsilon}}_f \; = \; l_c \; \| \langle \underline{\underline{\boldsymbol{m}}} \rangle \| \; \dot{\lambda} \tag{44}$$

where the McCauley operator extracts only the tensile components of the plastic potential surface gradient $\underline{\underline{\boldsymbol{m}}}$.
The characteristic length l_c in the PDM is determined in terms of the actual confinement level and of concrete quality.

4.4 Plastic Potential

A non associative flow rule is adopted by defining a plastic potential introducing a modification on the dependence of the loading/unloading surfaces on the hydrostatic coordinate $\bar{\xi}$.
The plastic potential surfaces in hardening g_h and in softening g_s are mathematically described as follows

$$g_{h(k)} = \begin{cases} g^{cone}_{h(k)} = Ar^2\bar{\rho}^2 + B_c r\bar{\rho} + \eta_{o(\bar{\xi})} C\left(\bar{\xi} - \bar{\xi}_{1(k)}\right) + C\bar{\xi}_{1(k)} - 1 = 0 \quad if \quad \bar{\xi} \leq \bar{\xi}_{1(k)} \\ g^{cap}_{h(k)} = \dfrac{[\eta_{o(\bar{\xi})}(\bar{\xi} - \bar{\xi}_{1(k)}) + (\bar{\xi}_{1(k)} - \bar{\xi}_{cen(k)})]^2}{a^2_{(k)}} + \dfrac{r^2\bar{\rho}^2}{b^2_{(k)}} - 1 = 0 \quad if \quad \bar{\xi} > \bar{\xi}_{1(k)} \end{cases} \tag{45}$$

$$g_{s(c)} = Ar^2\bar{\rho}^2 + B_c r\bar{\rho} + \eta_{o(\bar{\xi})} C\left(\bar{\xi} - \bar{\xi}_1\right) + C\bar{\xi}_1 - c = 0 \tag{46}$$

The non associative parameter η_o is evaluated in terms of concrete quality and of the hydrostatic normalized stress $\bar{\xi}$ as follows

$$\eta_o = t_1 \exp\left(t_2\, x^{t3}\right) + t_4 \quad with \quad x = \begin{cases} \bar{\xi}_{vertex} - \bar{\xi} & \text{if} \quad \bar{\xi} \leq \bar{\xi}_t \\ \bar{\xi}_{vertex} - \bar{\xi}_t & \text{if} \quad \bar{\xi} > \bar{\xi}_t \end{cases} \tag{47}$$

and t_i, internal model parameters.

5 FAILURE MODES AND TYPES PREDICTIONS WITH THE PDM

In this section a localization analysis performed based on the PDM previously described is presented. For this purpose, the localization condition defined by Eq. 14 is checked.
Unit vector $\underline{\boldsymbol{N}}$ defining the normal to the potential failure plane is expressed in terms of spherical angles as

$$(n_1, n_2, n_3) = (cos\varphi\, cos\varphi^{'}\,,\; cos\varphi\, sin\varphi^{'}\,,\; sin\varphi) \tag{48}$$

Angle φ is the one formed between the normal to the plane and the direction of the principal stress σ_I in the plane defined by $[\sigma_I, \sigma_{III}]$ (being $\sigma_I > \sigma_{II} > \sigma_{III}$), and angle $\varphi^{'}$, so-called out of plane, the angle formed between the normal to the plane and the direction of the principal stress σ_I in the plane defined by $[\sigma_I, \sigma_{II}]$. Then, in all cases, the results are plotted in terms of the inclination of the normal to the failure surface with respect to an horizontal plane, indicating this angle as α. The analysis is performed for three concrete strengths: $f_c^{'}$= 30 (normal strength concrete: NSC), 70 (medium strength concrete: MSC) and 120 MPa (high strength concrete: HSC), and its medium β_P values= 0.060, 0.230 and 0.803 respectively. Poisson$'$s ratio was considered 0.20, and Young's modulus was considered 26000, 35000 and 40000 MPa respectively. A maximum coarse aggregate size of 2cm was considered.
The results for uniaxial compression, using the analytical localization method are presented in Fig. 3, for three load states: at 80% of the peak load, at 90% of the peak load and at the peak load. Observing these results, the following conclusions may be extracted:
1- At 80% of the peak load, the HSC is still undamaged, while the NSC and the MSC already show a certain level of damage.

2- At 80% of the peak load, the potential failure plane of the MSC is more vertical than the one of the NSC.

3- At 90% of the peak load, the HSC shows damage, with a potential failure plane more vertical than the one of the MSC which in turn is more vertical than the one of the NSC.

4- At the peak load, the localization condition is not reached, and therefore, the failure type is diffuse.

5- In Fig. 4 where a zoom view of the minimum value of the plot in Fig. 3c) is presented, it may be observed that the potential localization planes at the peak are still more vertical for HSC. Although localization is not detected, this fact allows to interpret that HSC, according with the PDM, are less stable than NSC.

6- The direction of the potential failure planes only deviates between 0 to 30^o from the direction of the applied load, indicating a possible failure mode between shear and mixed failure types. The results agree with general observations detected in experimental tests. (See a.o. van Mier (1997), Lee (2002), etc.).

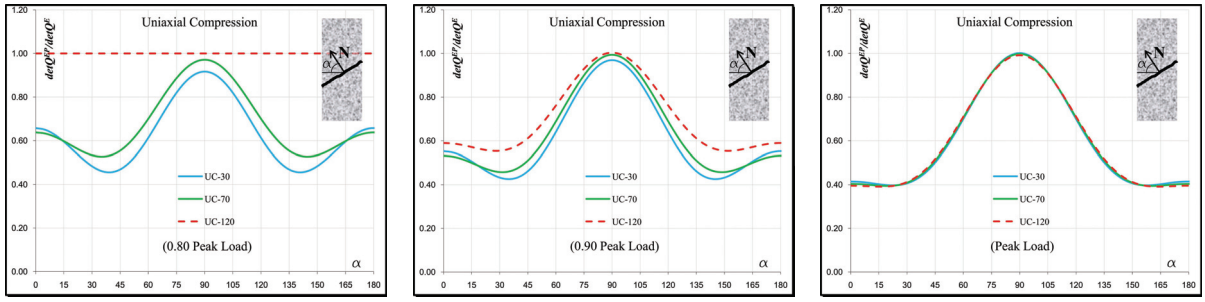

(a) (b) (c)

Figure 3: Uniaxial Compression (Lode Angle 60^o) (a) 0.80 Peak; (b) 0.90 Peak; (c) Peak

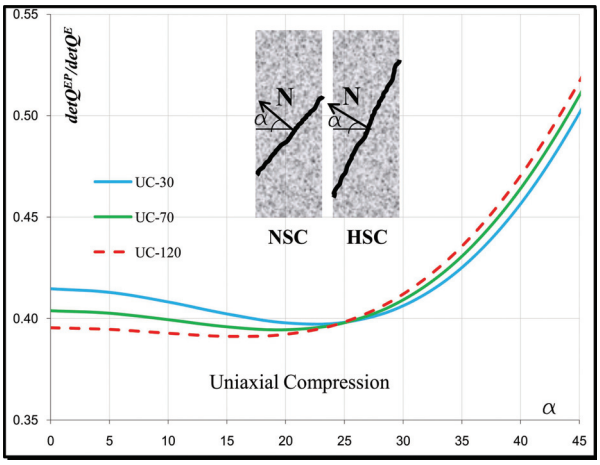

Figure 4: Uniaxial Compression - Preferential failure direction for different concrete qualities

Then, in Fig. 5 the results for uniaxial compression applying the geometrical method are plotted. It may be observed the coincidence of these results with those in Fig. 3, leading to

analogous failure modes and to the same angles of the potential failure planes.

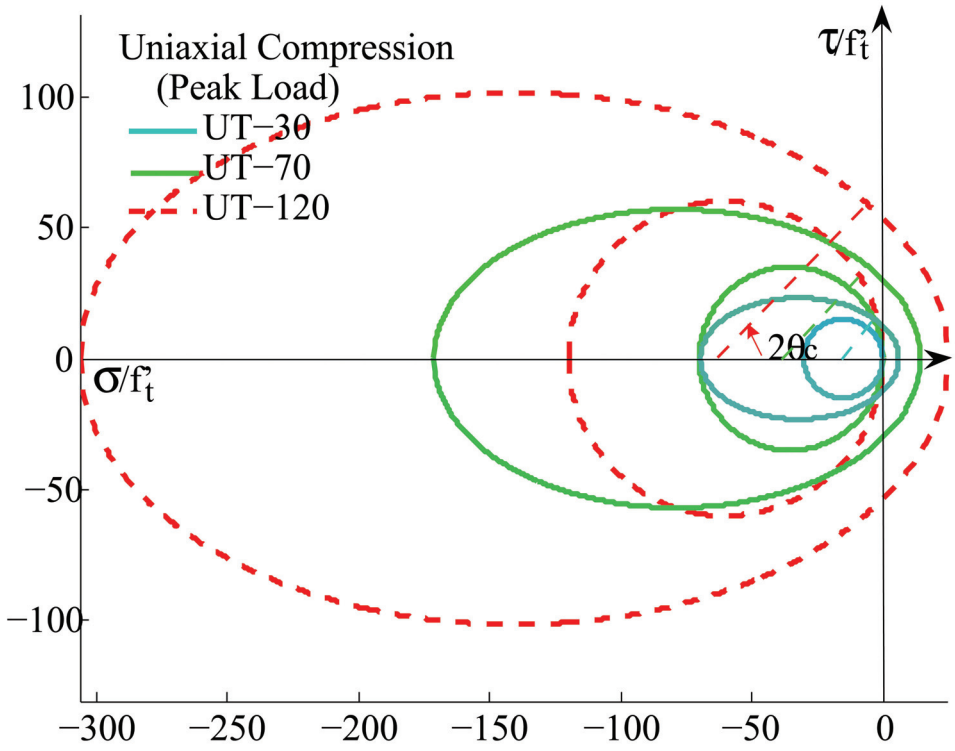

Figure 5: Uniaxial Compression - Preferential failure direction for different concrete qualities

6 CONCLUSIONS

In this work the failure characteristics of concretes of different qualities is presented based on the failure modes predicted by the Performance Dependent Model for Concretes of Arbitrary Strengths, a constitutive model recently developed in order to capture the mechanical failure behavior both of normal and high strength concretes.

Some results corresponding to ongoing research are presented, considering three different concrete qualities, subjected to uniaxial compression. The discontinuous bifurcation condition is analyzed applying the analytical and the geometrical methods.

The results demonstrate that concrete quality has an important incidence on the failure features. Although for the case of uniaxial compression localization is not reached, the angles of the potential failure planes indicate that high strength concretes are considerably less stable than normal strength concretes.

Future research will extend the present analysis to other loading paths.

7 AKNOWLEDGMENTS

The authors gratefully acknowledge the partially financial support of this work by the Universidad de Buenos Aires (UBACYT 2010-2012 No. 20020090100139), by CONICET (PIP 112-200801-00707), and by the INTECIN and the Laboratory of Materials and Structures at the FIUBA, Argentina.

REFERENCES

Benallal A. On localization phenomena in thermo-elasto-plasticity. *Arch. Mech.*, 44:15–29, 1992.

Benallal A. and Comi C. Localization analysis via a geometrical method. *International Journal of Solids and Structures*, 33:99–119, 1996.

Etse G. *Theoretische und numerische untersuchung zum diffusen und lokalisierten Versagen in Beton*. Ph.D. thesis, University of Karlsruhe, Karlsruhe, Germany, 1992a.

Etse G. Numerical failure analysis of pull-out test. *Zeit. Angew. Math. und Mech.*, 4:158–161, 1992b.

Folino P. and Etse G. Endurecimiento a través de superficies con capa dependientes del grado de prestación del hormigón. *Mecánica Computacional*, XXVII:909–926, 2008.

Folino P. and Etse G. Elastoplastic constitutive model for concretes of arbitrary strength properties. In *EURO-C, Austria, 2010, ŞComputational Modelling of Concrete StructuresŤ, ISBN: 978-0-415-58479-1, Ed. CRC Press, London, UK, 129-136*. 2010.

Folino P. and Etse G. Validation of the performance dependent failure criterion for concretes. *ACI Materials Journal*, 108(3):261–269, 2011.

Folino P., Etse G., and Will A. A performance dependent failure criterion for normal and high strength concretes. *ASCE Journal of Engineering Mechanics*, 135(12):1393–1409, 2009.

Hadamard J. *Leçons sur la Propagation des Ondes et les Equations de Hydrodynamique*. Librairie Scientifique A. Hermann, Paris, France, 1903.

Hill R. Acceleration waves in solids. *Journal of Mechanics and Physics of Solids*, 10:1–16, 1962.

Kang H. and Willam K. Localization characteristics of triaxial concrete model. *ASCE Journal of Engineering Mechanics*, 125(8):941–950, 1999.

Lee I. *Complete stress-strain characteristics of high performance concrete*. Ph.D. thesis, New Jersey Institute of Technology, New Jersey, US, 2002.

Liebe T. Analytical and geometrical representation of localization analysis of curvilinear drucker-prager elastoplasticity. 1998. Dipl. thesis, Technical report, University of Hanover, Germany.

Ortiz M. An analytical study of the localized failure modes of concrete. *Mechanics of Materials*, 6:159–174, 1987.

Ottosen S. and Runesson K. Properties of discontinuous bifurcation solutions in elasto–plasticity. *International Journal of Solids and Structures*, 27:401–421, 1991.

Perić D. Localized deformation and failure analysis of pressure sensitive granular materials. 1990.

Pijaudier-Cabot G. and Benallal A. Strain localization and bifurcation in a non-local continuum. *International Journal of Solids and Structures*, 13:1761–1775, 1993.

Rice J. The localization of plastic deformation. In *Theoretical and Applied Mechanics (Proceedings of the 14th International Congress on Theoretical and Applied Mechanics, Delft, The Netherlands, ed. W.T. Koiter),Vol. 1, NorthHolland Publishing Co.*, pages 207–220. 1976.

Rudnicki J. and Rice J. Condition for the localization of deformation in pressure-sensitive dilatant material. *Journal of Mechanics and Physics of Solids*, 23:371–394, 1975.

Truesdell C. and Toupin R. *The Classical Field Theories*. Handbuch der Physik, ed. by Fl´ugge, Vol. III/1, Springer-Verlag, Berlin, Germany, 1960.

van Mier J. *Fracture Processes of Concrete*. CRC Press, Boca Raton, Florida, US, 1997.

Vrech S. *Simulación computacional de procesos de falla localizada basada en teoría de gradi-*

entes. Ph.D. thesis, Universidad Nacional de Tucumán, Tucumán, Argentina, 2007.

Willam K. Constitutive models for engineering materials. *Encyclopedia of Physical Science & Technology*, 3:603–633, 2002.

Willam K. and Warnke E. Constitutive model for the triaxial behavior of concrete. In *Intl. Assoc. Bridge Struct. Engrg.,Report 19, Section III, Zurich, Switzerland*, pages 1–30. 1974.

Xie J., Elwi A., and Mac Gregor J. Mechanical properties of three high-strength concretes containing slica fume. *ACI Materials Journal*, 92(2):135–145, 1995.